

Investigating the Planetary Dynamics Induced by the Wide Stellar Companion to Boyajian’s Star

LOGAN PEARCE

1. INTRODUCTION

In the mid 2010’s, citizen scientists in the Planet Hunters project (Fischer et al. 2012) flagged the *Kepler* light curve of the Kepler Input Catalog object KIC 8462852 as being “bizarre”, “interesting”, and a “giant transit” (Boyajian et al. 2016, hereafter B16). The light curve, reported in B16, exhibits large, possibly aperiodic dips of a variety of shapes, some as deep as 20%, which is abnormally deep for a transit. Figure 1 displays the normalized light curve for the entire 4-year *Kepler* observation window, with interesting features marked in blue. The light curve also contained a short period oscillation consistent with the 0.88 day rotation period of the star, and a long period oscillation of \sim 10-20 days, which is present in some of the Kepler observations, but not all, as shown in Figure 2. Additionally, Montet & Simon (2016) showed that the light curve also exhibits a gradual dimming trend throughout the *Kepler* observation, and Simon et al. (2018) showed that this is part of an even longer-term dimming of \sim 6.3 mmag yr⁻¹, with some irregular brightening events. The unique and unexplained nature of the light curve led to a flood of scientific and public interest, and the nickname “Boyajian’s Star” or “Tabby’s Star”.

Many possibilities have been investigated to attempt to explain the unique light curve. So far, no physical processes satisfactorily explain all the unique features. Some explanations such as recent cataclysmic dust-generating events (Marengo et al. 2015), massive debris disks (Thompson et al. 2016), close-in obscuring material or YSO-like behavior (Lisse et al. 2015), and instrumental effects (B16) have already been ruled out as explanations. Public interest in this star was ignited when alien megastructures were posited (Wright et al. 2016), however SETI searches and multi-wavelength observations have eliminated this intriguing possibility (alas, it is not removed from the public consciousness however, as pop-sci alien articles still appear whenever new science about this star is published). The break-up of exocomets or planetesimals on eccentric orbits was preferred given the observations (Thompson et al. 2016), although Bodman & Quillen (2016) showed this idea does not fully explain all the dips, nor the apparent long term dimming trend (Montet & Simon 2016). Boyajian et al. (2018) showed that post-Kepler observations are consis-

tent with optically thin dust and intrinsic variations of the star, however Martínez González et al. (2019) found no clear evidence of comets and evidence for clumps of optically-thick material within the thin dust.

In Pearce et al. 2021, hereafter P21, we showed that a near-by star at \sim 2''(880 AU) separation, first identified as a candidate companion in B16, is in fact a gravitationally-bound wide binary companion to Boyajian’s Star. Figure 3 reproduces Figure 1 of that work, and shows a Keck/NIRC2 image of the primary KIC 8462852 A (Boyajian’s star, labelled ‘A’), the secondary KIC 8462852 B (labelled ‘B’), and two candidate companions which we showed to be unassociated with the system. Table 1 reproduces Table 2 of P21 and displays properties of the system. The 5 year observational baseline of P21 was not sufficient to place any meaningful limits on the orbit of the binary. A face-on, circular orbit would give this system a period of 18,600 years, for which a linear relative velocity would be resolvable in the next \sim 10-20 years with 1 mas astrometric precision, and acceleration in \sim 450 years, making it difficult to place meaningful constraints on the current orbit of the binary.

Given the current wide separation (\sim 880 AU) between the two components, KIC 8462852 B is unlikely to be currently influencing the light curve of KIC 8462852 A, and does not immediately explain any of the unique features (despite pop-sci claims to the contrary¹). However, the presence of a wide stellar perturber in the system would have influenced the dynamics of objects in orbit around KIC 8462852 A throughout its 1.2 Gyr history. Simulations (e.g Kaib et al. 2011, 2013; Correa-Otto & Gil-Hutton 2017) have shown that objects on wide orbits (\sim 1000 AU) from their host stars are perturbed by the galactic potential and flybys of other stars, and that this perturbation can induce high eccentricity, low periastron states. Tokovinin & Kiyaeva 2016 found the average eccentricity of wide binary systems (WBS; period = 10^5 - 10^6 days) of nearby ($<$ 67 pc) solar-type binaries to be 0.59, suggesting high-eccentricity orbits are relatively common. For WBS, high eccentricity orbits can propagate to eccentricity disturbances of planetary sys-

¹

<https://www.wionews.com/science/scientists-resolve-mystery-of-boyajians-star-say-alien-megastructure-is-not-alien/>

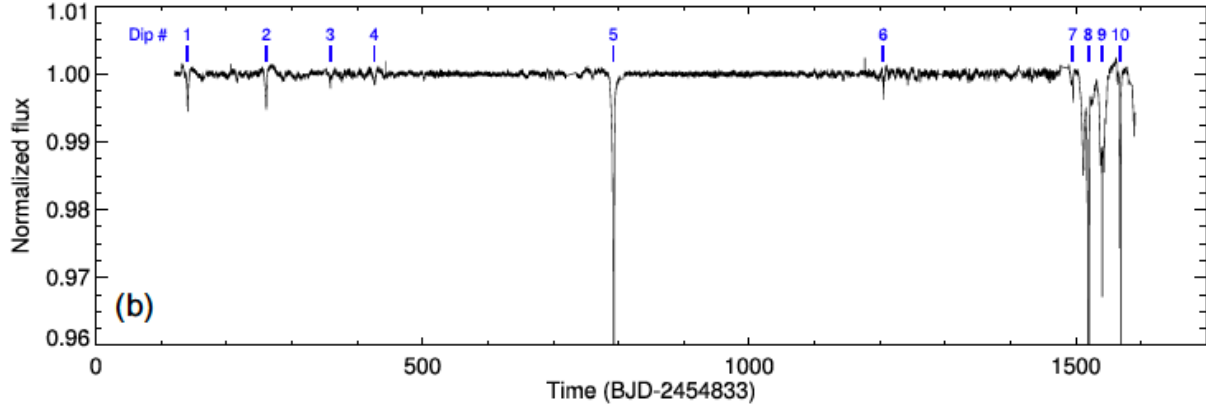


Figure 1. A portion of Figure 1 of B16 showing the normalized light curve of KIC 8462852 for the entire 4-year *Kepler* mission. Interesting features are indicated by blue numbers. Dip 5 and 8 are $\gtrsim 20\%$ deep. Dips 6 and 9 are similar shape but very different depths and durations. Dips 1,2,3,4, and 6 are similar shapes but different depths and durations, and do not appear to be periodic during the *Kepler* observation window. The shapes, depths, and aperiodicity of these dips are not easily explained by a physical explanation.

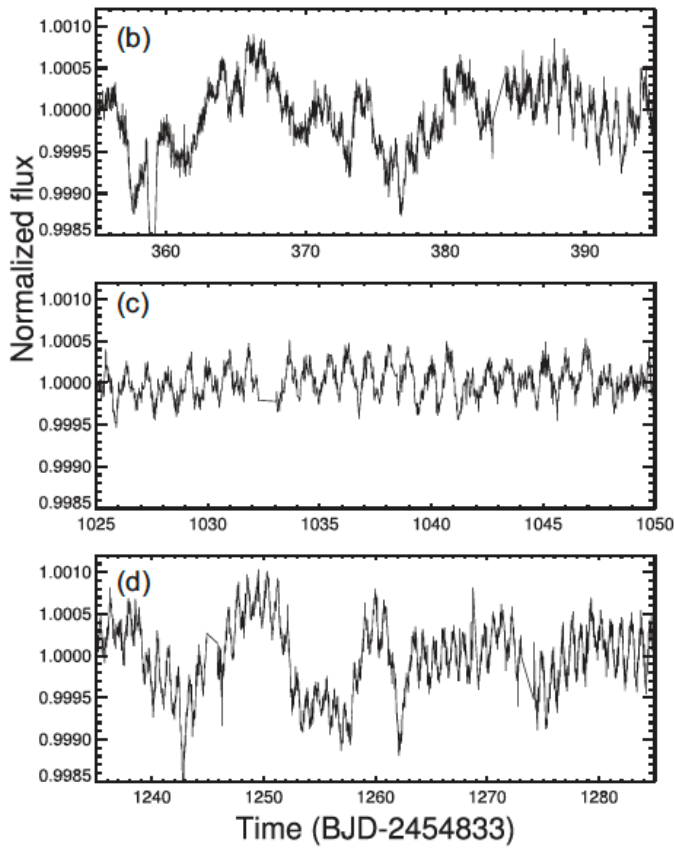


Figure 2. A portion of B16 Figure 4 showing the normalized light curve of KIC 8462852 for different time periods of *Kepler* observation window. The short term periodicity of the star's 0.88 day rotation period is seen in all three panels. The long term periodicity ($\sim 10-20$ days) is seen in all panels except 'c'.

Table 1. System and Stellar Properties for KIC 8462852 AB

Property		Ref
Distance (pc)	$451.0^{+4.9}_{-4.8}$	1
ρ (mas)	1951.48 ± 0.23	2
ρ (AU)	880 ± 10	2
PA ($^{\circ}$)	96.063 ± 0.004	2
<i>KIC 8462852 A</i>		
Proper Motion	$\mu_{\alpha} = -10.422 \pm 0.040$	3
(mas yr $^{-1}$)	$\mu_{\delta} = -10.288 \pm 0.041$	3
Luminosity (L_{\odot})	4.3 ± 0.3	2
Mass (M_{\odot})	1.36 ± 0.05	2
Radius (R_{\odot})	1.51 ± 0.04	2
T_{eff} (K)	6750 ± 120	4
SpT	F3V	3
Age (Gyr)	~ 1.2	2
J (mag)	10.763 ± 0.021	5
H (mag)	10.551 ± 0.019	5
K (mag)	10.499 ± 0.020	5
<i>KIC 8462852 B</i>		
Mass (M_{\odot})	0.44 ± 0.02	6, 2
Radius (R_{\odot})	0.45 ± 0.02	2
T_{eff} (K)	3720 ± 70	2
SpT	M2V	4

References—(1) Bailer-Jones et al. (2018) (2) Pearce et al. (2021) (3) Gaia DR2 (Gaia Collaboration et al. 2016, 2018); (4) Boyajian et al. (2016); (5) 2MASS (Skrutskie et al. 2006); (6) Mann et al. (2019)

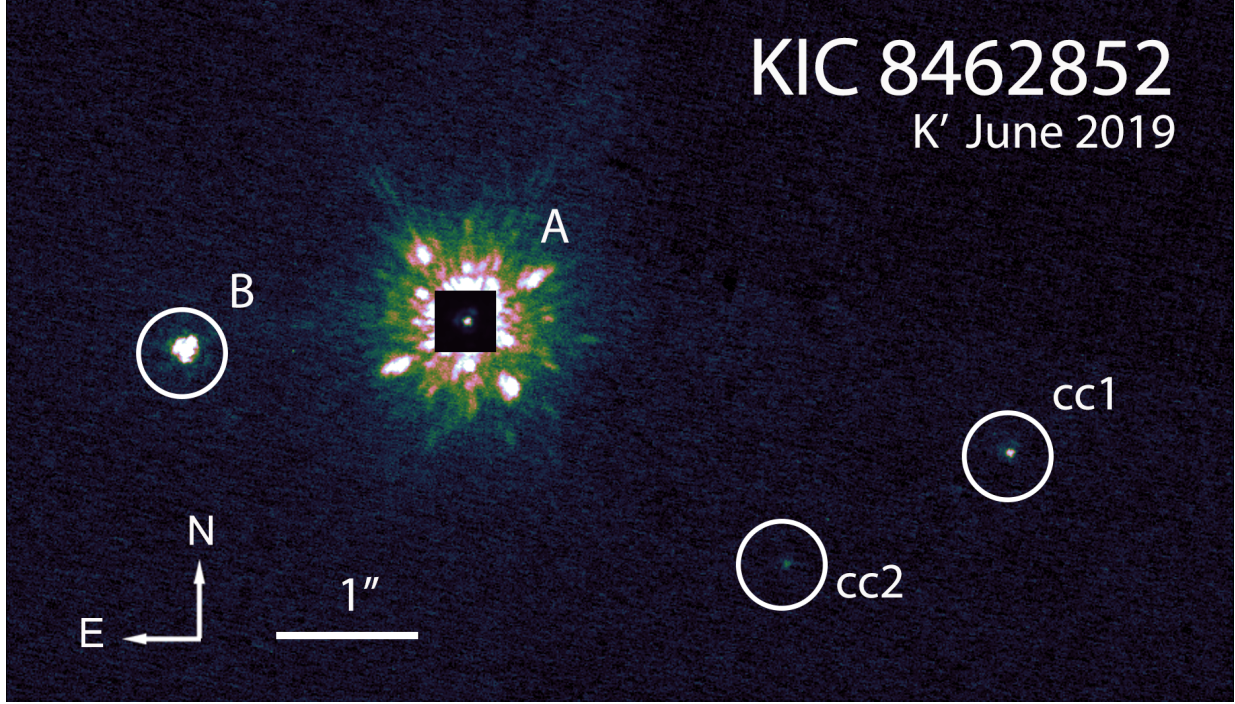


Figure 3. Figure 1 of Pearce et al. 2021. Keck/NIRC2 adaptive optics image of KIC 8462852 A, B, and two candidate companions, shown in log stretch to emphasize the faint candidate companions. The primary, KIC 8462852 A, is shown inside a linear stretched box to avoid saturation. The secondary, labeled B, is located $2''$ to the east. The two candidate companions (cc1 and cc2) are shown in that work to be unassociated with the system.

tems (Zakamska & Tremaine 2004). Correa-Otto & Gil-Hutton 2017 found that 10-30% of their simulated WBS had gravitational disruption in the planetary region due to the influence of the galactic potential and evolution of the secondary’s orbit. Bazsó & Pilat-Lohinger 2020 showed that the presence of a giant planet around one of the stars induced secular resonances and chaotic regions interior to the giant planet. All of this points to the wide companion exerting a disruptive influence on the planetary region, and that KIC 8462852 B would have contributed to the evolution of the environment around KIC 8462852 A, likely making it a dynamically evolving and disruptive environment.

This work aims to explore the influence of the wide companion on objects in the planetary region around KIC 8462852 A, assuming that KIC 8462852 B is currently in a high-eccentricity, low periastron state. In Section 2 I outline the methodological approach I took to this problem and describe the set up of simulations. In Section 3 I describe the approach I took to analyzing the simulation results. In Section 4 I describe the results of the analysis. In Section 5 I discuss the implications of the results for the Boyajian’s Star system, and in Section 6 I discuss how this study could be improved to provide more meaningful results.

2. METHOD

2.1. Wide Binary Orbit

A simulation from Kaib et al. 2013 Figure 1 is reproduced in Figure 4, with the secondary’s periastron given by the solid black line, semi-major axis by the dotted black line, and simulated planets by the colored lines. In this simulation, the secondary oscillates between periods of close and wide periastron, with the first close periastron passage occurring at about 1 Gyr. These close periastron passages eventually eject both Uranus and Neptune analogs from the system. The Boyajian’s Star system age is ~ 1 Gyr, meaning it is possible that is in a similar close-periastron phase today.

Using this Kaib et al. 2013 simulation as a suggestion for the Boyajian’s Star system configuration, I simulated the WBS using the open-source python package `rebound` (Rein & Liu 2012). Figure 4 shows the semi-major axis $a \approx 9000$ AU, and periastron $r_p \approx 100$ AU at 1 Gyr, which represents a possible WBS system orbit with eccentricity $e = 0.989$. To sample a set of possible orbits of varying eccentricity, I also models the binary orbit using $a = 7000$ AU and $a = 2000$ AU, and $r_p = 200, 300, 500$ AU, creating a set of 12 possible binary orbit configurations.

For each binary configuration, I fit for a posterior of possible orbits which matched the semi-major axis, periastron, and current plane-of-sky separation using the

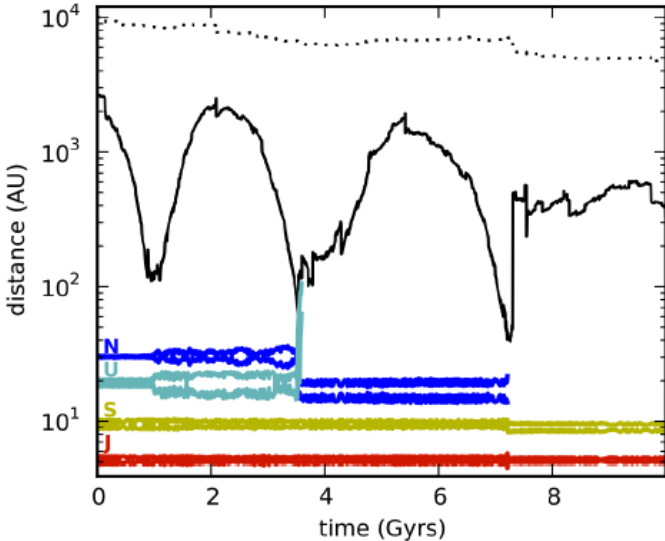


Figure 4. A reproduction of Kaib et al. (2013) Figure 1 showing the result of a simulation of a wide binary perturbed by the galactic potential and stellar flybys over a 10 Gyr period. The secondary periastron is given by solid black line, and semi-major axis by the dotted black line. A Jupiter (red), Saturn (yellow), Uranus (green), and Neptune (blue) analog were included around the primary. The secondary passes through periods of close periastron passage, the first occurring around 1 Gyr, which perturbs the orbits of the planets and eventually ejects both Neptune and Uranus from the system.

Orbits for the Impatient (OFTI) methodology (Blunt et al. 2017). Briefly, OFTI randomly samples four orbital parameters from priors (eccentricity: uniform $[0,1.0]$, inclination: $\cos(i)$ uniform on $[-1,1]$, argument of periastron: uniform on $[0,2\pi]$, orbit phase: uniform on $[0,1]$) to create a trial orbit, scales the semi-major axis of the trial orbit and rotates the longitude of nodes to match the observed position, then performs an accept/reject step by comparing the trial orbit’s probability to a uniform random number on $[0,1]$. For this implementation, the scaling step is unnecessary because we are setting the semi-major axis to our desired value. Trial orbits were generated in batches of 10,000, and trials were repeated until 100,000 orbits were accepted, which formed the posterior distribution of likely orbits for each of the 12 configurations. (For more detail on my implementation of OFTI, see Pearce et al. 2019).

Figure 5 displays the prior and posterior distribution from OFTI of orbital elements consistent with semi-major axis $a = 9000 \pm 20$ AU and periastron $r_p = 100 \pm 2$ AU and current observed plane of the sky position (uncertainties on a and r_p are arbitrary and set to give a reasonable range of allowed orbits). The orbital parameters are: semi-major axis (sma), eccentric-

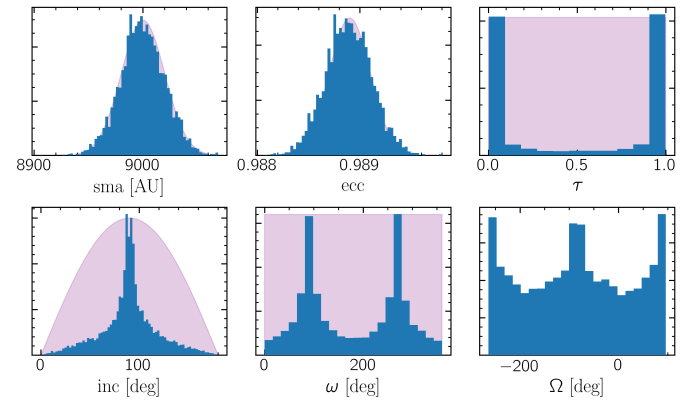


Figure 5. Posterior of orbital parameters for OFTI fit with current position of KIC 8462852 B relative to A, with semi-major axis $a = 9000 \pm 20$ AU and periastron $r_p = 100 \pm 2$ AU. Parameters are: semi-major axis (sma), eccentricity (ecc), inclination relative to plane of the sky (inc), orbit phase of observation (τ), argument of periastron (ω), and longitude of nodes (Ω). Prior distribution is shown in purple for each parameter, posterior distribution shown in blue. No prior exists for longitude of nodes due to OFTI fitting process.

ity (ecc), inclination relative to plane of the sky (inc), orbit phase of observation (τ), argument of periastron (ω), and longitude of nodes (Ω). The reference plane is the plane of the sky (edge-on orbit: $\text{inc} = 90^\circ$), and reference direction is north declination. This reference system is used for all orbital elements discussed in this work.

2.2. Planets

To test the effect of the presence of a giant planet around the primary, I provided the ability to simulate a Jupiter analog. If desired, a particle was initialized around the primary with Jupiter’s mass ($1 \times 10^{-3} M_\odot$), with semi-major axis of 5 AU, inclination 90° so that it was always aligned edge-on with respect to the observer, longitude of nodes of 0° , and a random argument of periastron. No other planets were used in this simulation suite.

2.3. Test Particles

To investigate the binary’s effect on the environment around the primary, I established three different categories of test particles (TP) which were initialized around the primary in `rebound`: Exo-Asteroid Belt, Exo-Kuiper Belt, and a Uniform Distribution of TPs with respect to semi-major axis. The three categories and their prior distributions are summarized in Figure 6. The prior on each parameter is loosely adapted and simplified from observational results. The inclination prior is multiplied by a factor of $(1/3)$ to capture the fact that inclinations extend roughly no more than 30° above and

Exo-Asteroid Belt (AB)	<ul style="list-style-type: none"> SMA: Unif on [2.1,3.3] AU Diameter: Power law, index = -2 Mass derived from Diameter assuming density = 1.25 g/cm³ Ecc: Unif on [0.0,0.3] Inc: $\cos(i)^*(1/3)$ Uniform on (-1,1) rad
Exo-Kuiper Belt (KB)	<ul style="list-style-type: none"> SMA: Unif on [30,55] AU Diameter: Power law, index = -4 Mass derived from Diameter assuming density = 1.25 g/cm³ Ecc: Linearly decreasing on [0.0,0.4] Inc: $\cos(i)^*(1/3)$ Uniform on (-1,1) rad
Uniform Distribution (U)	<ul style="list-style-type: none"> SMA: Unif on [0.5,30] AU Diameter: Power law, index = -4 Mass derived from Diameter assuming density = 1.25 g/cm³ Ecc: Unif on [0.0,0.3] Inc: $\cos(i)^*(1/3)$ Uniform on (-1,1) rad

Figure 6. The three categories of test particles simulated in this work and the distributions their orbital parameters are drawn from. Priors are adapted loosely from observational results. Each test particle is also assigned a mass and radius, to investigate effects of transits.

below the ecliptic plane. Each test particle was also assigned a mass, from which radius was derived, to enable investigation of transiting objects.

For each category of test particle, the longitude of ascending node (Ω) could be taken from two different configurations. To align each particle in a “disk”, Ω was confined to $\Omega = 0.0$, so that each object was oriented in the same direction in the plane of the sky. For a more chaotic, “non-disk” configuration, Ω was drawn from a uniform prior on $[0,2\pi]$ to produce a random orientation. I ran each binary orbit configuration in both “disk” and “non-disk” configurations, leading to 24 total simulation configurations (12 binary orbit configurations, 2 disk/non-disk configurations).

Each test particle is initiated as a `rebound` “semi-active” particle, which means the particles are influenced by the active bodies (the two stars and any planets if present) but not each other, even though they have been assigned a mass value. The test particles were allowed to collide and merge, in which case their masses were combined, and a new radius value was computed based on the new mass and density.

2.4. Simulations

A diagram of the simulation procedure is shown in Figure 7. One simulation set was run for each binary orbit configuration (12 total) and each “disk” vs “non-disk” configuration (2 total), yielding 24 total simulation sets. Each simulation set was run on the University of Arizona HPC Puma using 20 core processes. Each process acted as an independent realization of the script, and ran 30 simulations each, yielding 600 total simulations per simulation set. On each simulation, the process randomly selected a binary orbit from the OFTI posterior, selected a TP configuration (Exo-Asteroid Belt,

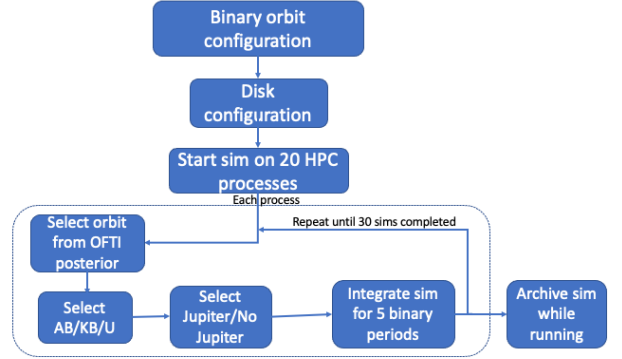


Figure 7. Diagram illustrating the simulation procedure used in this work. One simulation set was run for each binary orbit configuration and each “disk” vs “non-disk” configuration, yielding 24 total simulation sets, on the University of Arizona HPC using 20 core processes. Each process randomly selected a binary orbit from the OFTI posterior, and a test particle and planet configuration, and ran the sim for 5 binary periods. This was repeated 30 times per process, so each configuration was tested 100 times within a simulation set.

Exo-Kuiper Belt, or uniform distribution), and selected whether or not to initialize a Jupiter analog around the primary. The process then initialized and integrated the `rebound` simulation until 5 periods of the binary’s orbit had been completed, recording a simulation archive at set periods along the integration. This repeats until the process had completed 30 simulations. There are 6 possible simulation configurations the process selects from, so each configuration is tested 100 times per simulation set.

3. ANALYSIS

For each individual simulation, I determined which and how many of the 100 initial test particles remained in a bound orbit at the conclusion of 5 orbital periods, which I call “survivors”. This allowed me to see if the orbital elements of survivors had any commonalities among or between simulation sets. I determined, of the survivors, which and how many would transit, called “transiters”. For this work, I considered a survivor to be a transiter if any portion of the area of the circle described by its assigned radius intersected with the area of the primary’s disk at any point along the orbit. This is illustrated in Figure 8. If at any point the distance of the center of the particle from the center of the star (d) minus the radius of the particle (r_p) was less than the radius of the star (R_*), then I considered it to be a transiter. Finally, I determined if the secondary (B) and Jupiter (if present) survived, and their final orbital parameters.

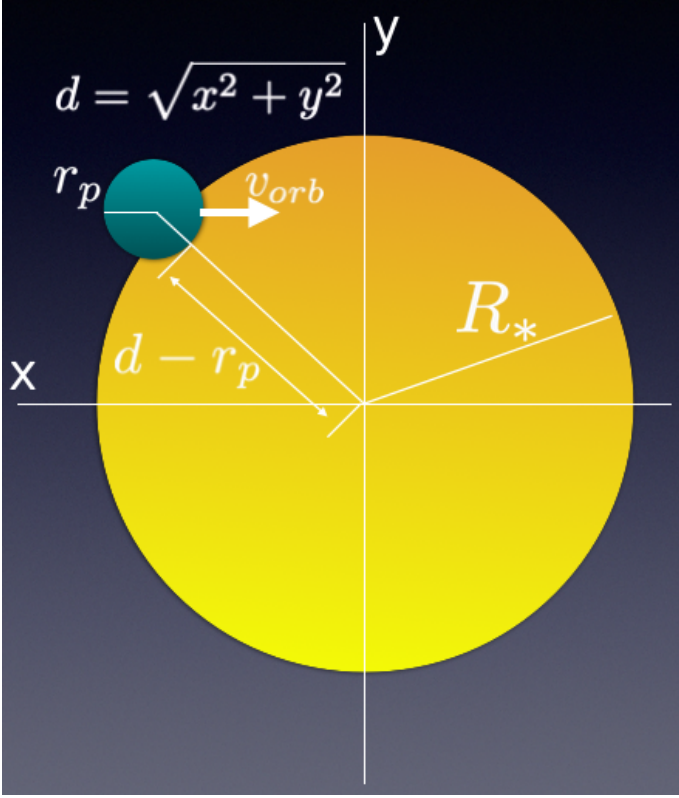


Figure 8. Illustration of the criterion for deciding if a survivor is a transiter in my simulation results. A survivor is considered a transiter if at any point along its orbit the distance from the center of the star to the center of the particle (d) minus the particle's radius (r_p) becomes less than the star's radius (R_*).

I do not expect B or Jupiter to be disrupted by the actions of the test particles, so there should only be perturbations on B due to Jupiter and vice versa. I predicted that the number of survivors would increase with increasing periastron, because I expected a more extreme secondary orbit would be more disruptive to the system. I predicted that the presence of a Jupiter in the system would decrease the number of survivors because it would induce resonances in the system that would not be present otherwise. I predicted that the survivors would have some commonalities to their orbits that were favorable for stability over the simulation period, such as alignment with the secondary's orbit.

4. RESULTS

Animations of selected simulations can be seen at:
<https://github.com/logan-pearce/PTSY595B>

4.1. Exo-Kuiper Belt

No Exo-Kuiper Belt test particle simulation had any survivors across all configurations. Additionally, Jupiter

was removed in every simulation, and the secondary merged with the primary in every single one. I cannot understand why this happened, as neither “active” body should have been influenced by the presence of the test particles. The fact that this was the result of every simulation is concerning. I can't explain why, because the Kuiper Belt simulations were initialized and executed in the same manner as all the others. Something went wrong in those simulations that is not readily apparent to me and I struggle to understand. For the remainder of this work I will discuss the Uniform Distribution and Exo-Asteroid Belt results only.

4.2. Survivors

Figure 9 displays the average number of survivors in simulations as a function of secondary's periastron distance for the three semi-major axes and disk/non-disk configurations for the Uniform Distribution TPs and Asteroid Belts, both with and without a Jupiter analog. Periastron distance is plotted on the x-axis, and increasing periastron distance corresponds to decreasing eccentricity for a given semi-major axis, since $r_p = a \times (1 - e)$. Contrary to expectation, there is no trend in increasing survivors with increasing periastron, with the exception of the Uniform Distribution without a Jupiter, where there is only a very slight trend. With the exception of the Uniform + Jupiter disk configuration, there does not seem to be a trend with increasing survivors with decreasing eccentricity. The $sma = 2000$ AU, periastron = 500 AU configuration has the lowest eccentricity ($e = 0.75$) and thus is the least extreme orbit, yet it does not appear to have more survivors on average than other configurations.

With the exception of the Asteroid Belt TP configuration, there were more survivors when in a disk than a non-disk configuration. This is due to there being fewer collisions between test particles when in a disk configurations. Collisions removed more particles from the system than the influence of the binary, and is a major flaw in this simulation design. I cannot explain why the non-disk configuration had more survivors than the disk for the Asteroid Belt simulations.

In all cases, the presence of a Jupiter analog in the system reduced the number of survivors, as expected.

The Asteroid Belt configuration retained overall fewer survivors than the Uniform Distribution of test particles. I believe this is due to more frequent collisions removing particles from the system rather than the influence of the binary, as the test particles are much closer to each other in Asteroid Belt configuration.

4.3. Number of Survivors as a Function of Binary Orbit

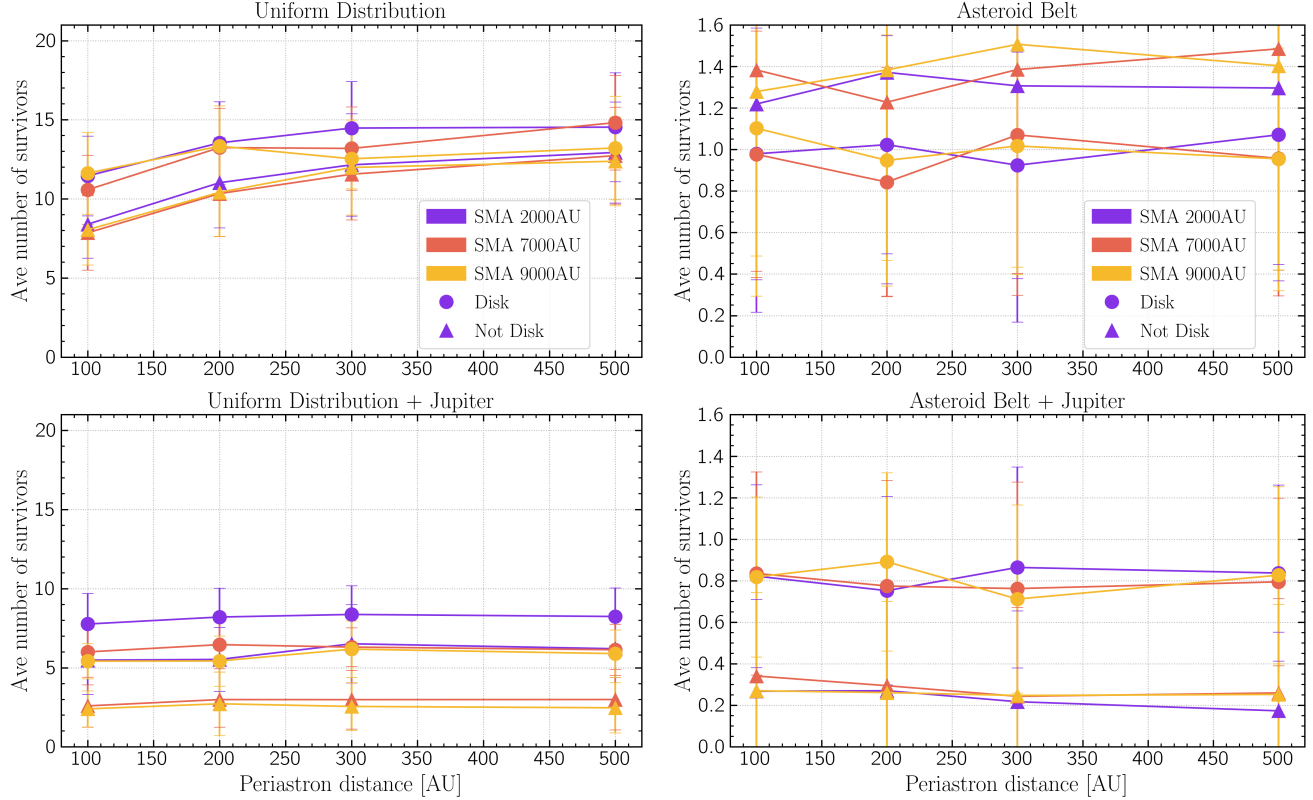


Figure 9. Average number of survivors as a function of the various configurations tested in this work. Periastron distance is plotted on the x-axis, so increasing periastron distance corresponds to decreasing secondary eccentricity for a given semi-major axis, since $r_p = a \times (1 - e)$. The colors denote semi-major axis; triangles indicate the “non-disk” test particle configuration, circles the “disk” configuration. Top panel: the Uniform TP configuration (left) and Exo-Asteroid Belt (right). Bottom panel: Uniform (left) and Asteroid Belt (right) with a Jupiter analog included in the system. We see no trend in number of survivors with decreasing eccentricity. With the exception of the Asteroid Belt, in all cases there were fewer survivors when in a non-disk configuration, because there are fewer TP collisions. In all cases, the presence of a Jupiter in the system decreased the number of survivors.

Figure 10 displays the number of survivors in a simulation as a function of the secondary’s inclination for that simulation for a selection of orbital configurations. Each simulation within that configuration is given as a purple dot, and includes all test particle configurations (AB, KB, U) and both Jupiter and non-Jupiter planet configurations. All selected simulation sets initialized test particles in a disk. Secondary alignment with the test particle disk ($\text{inc} \approx 90^\circ$) increased the number of survivors for only the most extreme case ($e = 0.989$), and for only some of the simulations. There is a very slight occurrence for this trend for other simulation sets where semi-major axis = 9000 AU and periastron = 100 AU. In other simulation sets this trend vanishes.

So there is only a very weak improvement in survivability when the secondary’s orbit is aligned with the disk around the primary, and only in the most extreme cases. The configuration of the secondary’s orbit had little impact on the amount of disruption of objects around the primary.

4.4. Survivor’s orbital parameters

Figure 11 displays the distribution of orbital elements of all survivors for simulation sets in the middle of eccentricities tested, where semi-major axis = 7000 AU and periastron = 300 AU, for both disk and non-disk configurations of Uniform Distribution test particles with no planet present. The initial distribution of the test particle orbital elements is shown in purple, and the final distribution shown in orange. The semi-major axis (sma) shows a depression of lower values for the non-disk configuration, which is not present in the disk configuration. The eccentricity and inclination shows greater deviation from initial values for the non-disk configuration than the disk configuration. I believe both of these observations are explained by greater number of mergers when in the non-disk configuration, especially when the orbits are smaller and test particles are more likely to encounter each other. These trends persist regardless of the binary orbit configuration.

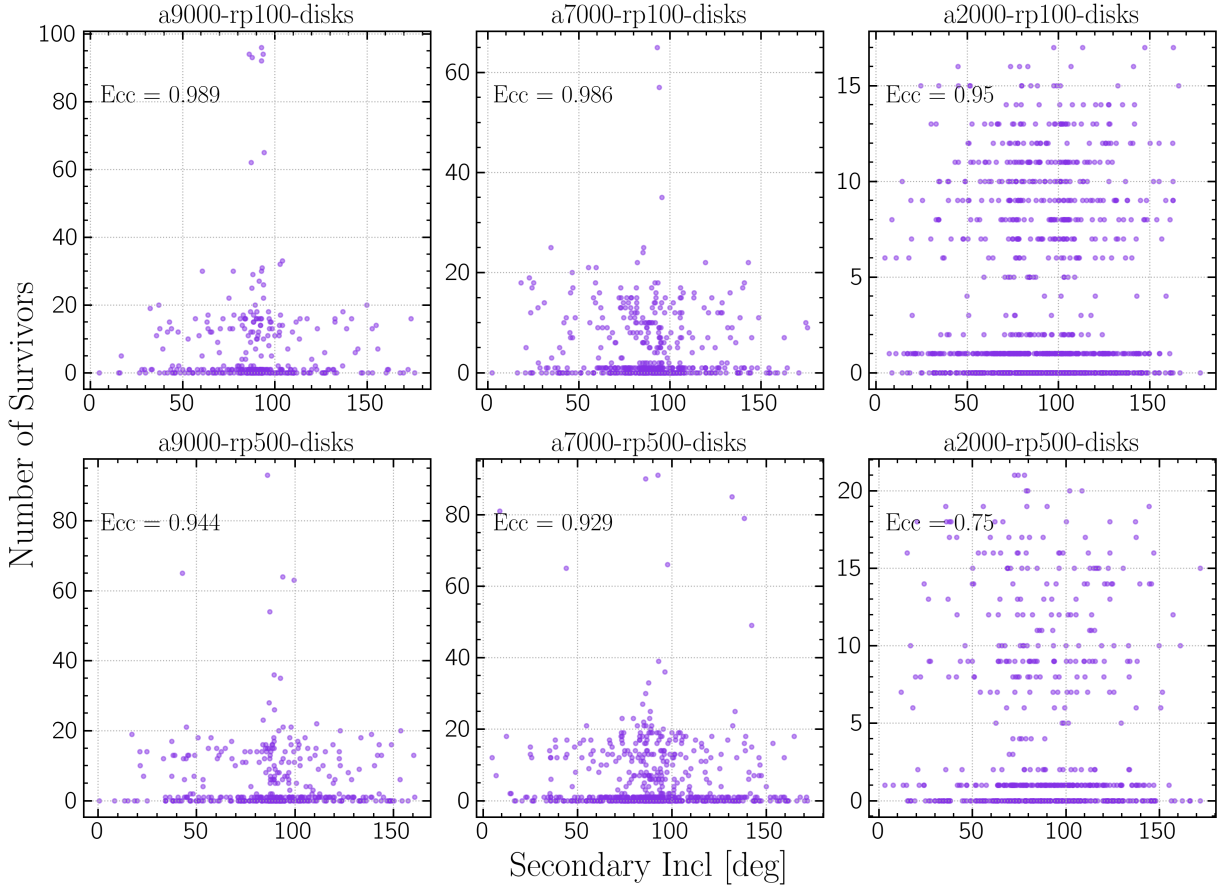


Figure 10. The number of survivors versus secondary's inclination for every simulation in a given secondary orbit configuration. The secondary orbit configuration is given at the top of each panel, where a = semi-major axis, rp = periastron, and disk = disk configuration. All selected configurations have test particles in disk configuration, and include the results for all test particle configurations (KB, AB, U) and both Jupiter and Non-Jupiter planet configurations. The eccentricity of the secondary's orbit is given within the panel. The number of survivors for a single simulation is given by a purple dot. We see the secondary's inclination alignment with the disk ($\text{inc} \approx 90^\circ$) increased the number of survivors only in the most extreme case ($e = 0.989$).

Figure 12 displays the same orbital element distributions for simulation sets with the Asteroid Belt configuration and a Jupiter analog present around the primary. We see the same trends in semi-major axis and eccentricity as Figure 11. However in the non-disk configuration, we see the majority of survivors have longitude of ascending node (lan) of either 0° or 180° , which is aligned or anti-aligned with the orbit of the Jupiter analog ($\text{lan} = 0^\circ$). So in this case only those objects aligned with the Jupiter's orbit survived.

4.5. Transits

For every simulation with survivors, some fraction were considered transits. However modeling the test particles as Asteroid- or Kuiper Belt-like is not a good model for reproducing the observed light curve for KIC 8462852 A. Objects of Asteroid Belt or Kuiper Belt radius distributions produce flux depths of or-

der $< 10^{-12}$ for KIC 8462852 A, corresponding to $10^{-5} R_{\text{Jup}}$. These would not be detectable by the *Kepler* mission. The modest dips in KIC 8462852 A's light curve (dips 1, 2, 6 of Figure 1), if produced by a single object, would require a radius of $\sim 1 R_{\text{Jup}}$. The presence of planets in the system is a possibility, but does not explain the abnormally deep dips or the irregular shaped dips, and neither does this simulation suite. This model is incapable of, and does not attempt to, replicate the observed light curve of KIC 8462852 A.

5. DISCUSSION

The majority of features observed in the results of these simulations can be explained by collisions and mergers of test particles in the `rebound` simulations. This is a major flaw in my simulation design and does not allow me to isolate the effects of the binary's influence. Additionally, this simulation is incapable of repro-

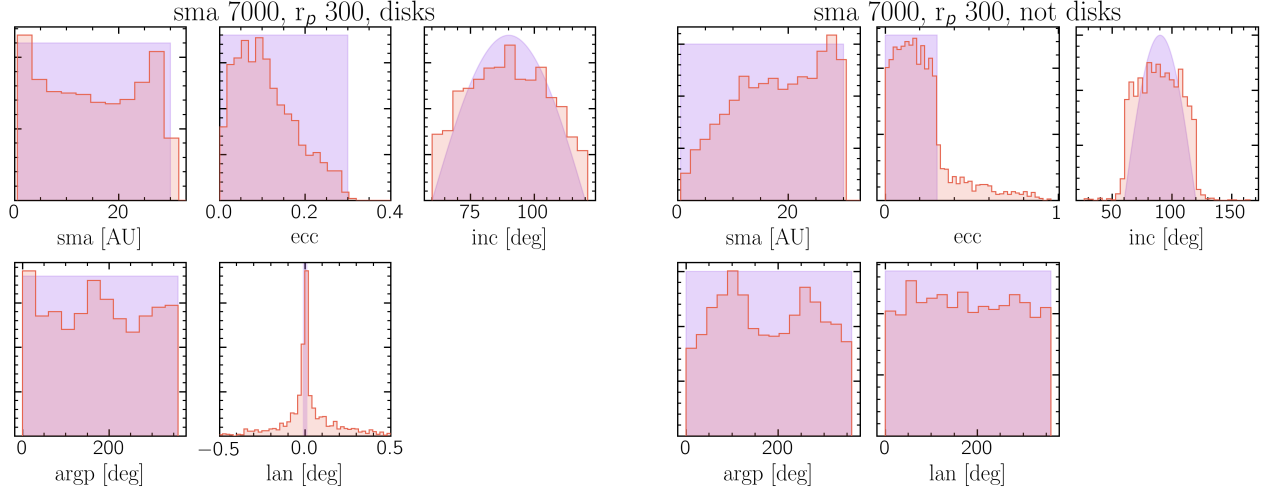


Figure 11. Prior distribution (purple) and final (orange) distribution of orbital elements of all surviving test particles in two simulation sets with semi-major axis = 7000 AU and periastron = 300 AU, with Uniform Distribution test particles in disk (left) and non-disk (right) configurations, and no Jupiter present.

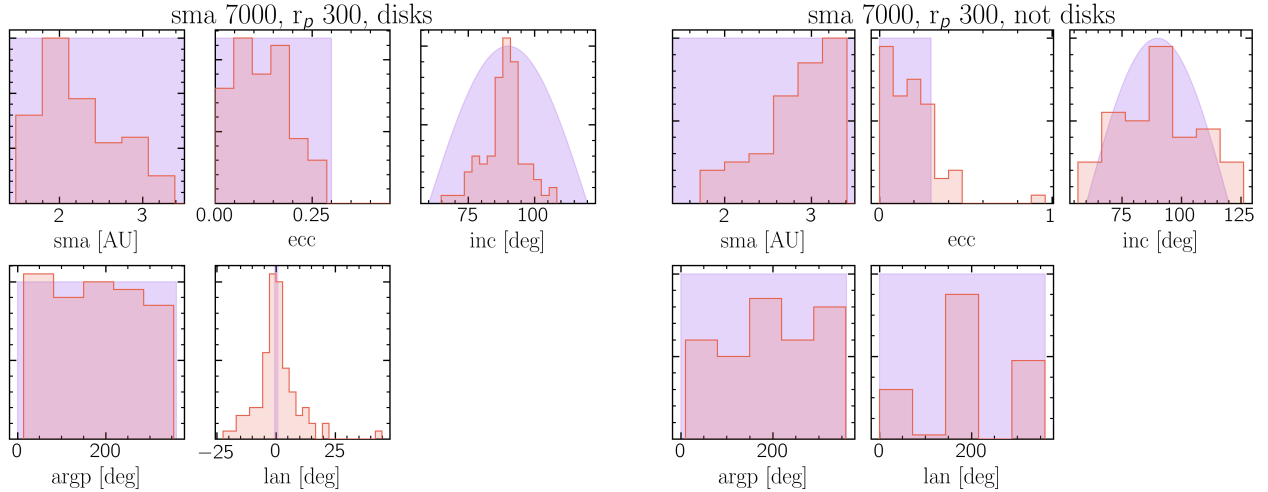


Figure 12. Prior distribution (purple) and final (orange) distribution of orbital elements of all surviving test particles in two simulation sets with semi-major axis = 7000 AU and periastron = 300 AU, with Asteroid Belt test particles in disk (left) and non-disk (right) configurations, and a Jupiter analog present around the primary.

ducing transit light curves, and is incapable of reproducing the observed light curve of KIC 8462852 A.

However I can say a few interesting things about the binary's influence. The presence of a planet around the primary did decrease survivors, as predicted and shown in [Bazsó & Pilat-Lohinger \(2020\)](#). Contrary to my prediction, the binary orbit configuration had little influence over the number of survivors, although that is a tentative conclusion as I was unable to isolate the influence of the binary alone. Object's alignment with the binary's orbit did improve survival, but only in the most

extreme cases ($e > 0.98$) which is not a likely configuration for the KIC 8462852 system.

6. IMPROVEMENT

The best way to improve the simulation suite and isolate the effect of the binary is to remove the ability for test particles to collide and merge. If test particles are invisible to each other, but not the active bodies in the simulation, the effect of the binary's and Jupiter's gravitational influence would be the only perturber on their initial orbital elements. I was unclear how to do this in

rebound initially, but I am sure it can be done within their infrastructure.

Next I would eliminate the Kuiper Belt category and expand the semi-major axis distribution beyond 30 AU to test the effect on wider bodies, but eliminate whatever the trouble was with the Kuiper Belt model. It would probably be best to eliminate the Asteroid Belt category as well to streamline the simulation sets and reduce the number of different permutations.

Finally I would increase the number of test particles to improve simulation of dust clumps and to improve survivor statistics. However this comes as a trade-off in integration time on the HPC, as it will be much more computationally expensive. A balance between compu-

tation time and number of test particles would have to be explored.

7. CONCLUSION

The presence of a wide stellar binary around KIC 8462852 A will influence the objects in orbit around it, however that influence may be minimal. The discovery of a wide binary companion should inform attempts to model the KIC 8462852 A to find a physical explanation for the enigmatic light curve, but it may not be much a factor in the current state or dynamical history of the environment around KIC 8462852 A. More work is needed to isolate the dynamical influence of the wide binary on the environment around KIC 8462852 A.

REFERENCES

- Bailer-Jones, C. A. L., Rybizki, J., Fouesneau, M., Mantelet, G., & Andrae, R. 2018, The Astronomical Journal, 156, 58.
<http://adsabs.harvard.edu/abs/2018AJ....156...58B>
- Bazsó, Á., & Pilat-Lohinger, E. 2020, The Astronomical Journal, 160, 2.
<https://doi.org/10.3847%2F1538-3881%2Fab9104>
- Bazsó, , & Pilat-Lohinger, E. 2020, The Astronomical Journal, 160, 2, publisher: American Astronomical Society.
<https://doi.org/10.3847%2F1538-3881%2Fab9104>
- Blunt, S., Nielsen, E. L., De Rosa, R. J., et al. 2017, The Astronomical Journal, 153, 229.
<http://adsabs.harvard.edu/abs/2017AJ....153..229B>
- Bodman, E. H. L., & Quillen, A. 2016, The Astrophysical Journal Letters, 819, L34.
<http://adsabs.harvard.edu/abs/2016ApJ...819L..34B>
- Boyajian, T. S., LaCourse, D. M., Rappaport, S. A., et al. 2016, Monthly Notices of the Royal Astronomical Society, 457, 3988.
<http://adsabs.harvard.edu/abs/2016MNRAS.457.3988B>
- Boyajian, T. S., Alonso, R., Amerman, A., et al. 2018, The Astrophysical Journal Letters, 853, L8.
<http://adsabs.harvard.edu/abs/2018ApJ...853L..8B>
- Correa-Otto, J. A., & Gil-Hutton, R. A. 2017, Astronomy and Astrophysics, 608, A116.
<http://adsabs.harvard.edu/abs/2017A%26A...608A.116C>
- Fischer, D. A., Schwamb, M. E., Schawinski, K., et al. 2012, Monthly Notices of the Royal Astronomical Society, 419, 2900.
<http://adsabs.harvard.edu/abs/2012MNRAS.419.2900F>
- Gaia Collaboration, Prusti, T., de Bruijne, J. H. J., et al. 2016, Astronomy and Astrophysics, 595, A1.
<http://adsabs.harvard.edu/abs/2016A%26A...595A...1G>
- Gaia Collaboration, Babusiaux, C., van Leeuwen, F., et al. 2018, Astronomy and Astrophysics, 616, A10.
<http://adsabs.harvard.edu/abs/2018A%26A...616A..10G>
- Kaib, N. A., Raymond, S. N., & Duncan, M. 2013, Nature, 493, 381.
<http://adsabs.harvard.edu/abs/2013Natur.493..381K>
- Kaib, N. A., Roškar, R., & Quinn, T. 2011, Icarus, 215, 491.
<http://adsabs.harvard.edu/abs/2011Icar..215..491K>
- Lisse, C. M., Sitko, M. L., & Marengo, M. 2015, The Astrophysical Journal Letters, 815, L27.
<http://adsabs.harvard.edu/abs/2015ApJ...815L..27L>
- Mann, A. W., Dupuy, T., Kraus, A. L., et al. 2019, The Astrophysical Journal, 871, 63.
<http://adsabs.harvard.edu/abs/2019ApJ...871...63M>
- Marengo, M., Hulsebus, A., & Willis, S. 2015, The Astrophysical Journal Letters, 814, L15.
<http://adsabs.harvard.edu/abs/2015ApJ...814L..15M>
- Martínez González, M. J., González-Fernández, C., Asensio Ramos, A., et al. 2019, MNRAS, 486, 236
- Montet, B. T., & Simon, J. D. 2016, The Astrophysical Journal Letters, 830, L39.
<http://adsabs.harvard.edu/abs/2016ApJ...830L..39M>
- Pearce, L. A., Kraus, A. L., Dupuy, T. J., et al. 2019, The Astronomical Journal, 157, 71.
<http://adsabs.harvard.edu/abs/2019AJ....157...71P>
- Pearce, L. A., Kraus, A. L., Dupuy, T. J., Mann, A. W., & Huber, D. 2021, The Astrophysical Journal, 909, 216, publisher: American Astronomical Society.
<https://doi.org/10.3847/1538-4357/abdd33>
- Rein, H., & Liu, S. F. 2012, A&A, 537, A128
- Simon, J. D., Shappee, B. J., Pojmański, G., et al. 2018, The Astrophysical Journal, 853, 77.
<http://adsabs.harvard.edu/abs/2018ApJ...853...77S>

- Skrutskie, M. F., Cutri, R. M., Stiening, R., et al. 2006,
The Astronomical Journal, 131, 1163.
<http://adsabs.harvard.edu/abs/2006AJ....131.1163S>
- Thompson, M. A., Scicluna, P., Kemper, F., et al. 2016,
Monthly Notices of the Royal Astronomical Society, 458,
L39.
<http://adsabs.harvard.edu/abs/2016MNRAS.458L..39T>
- Tokovinin, A., & Kiyaeva, O. 2016, Monthly Notices of the
Royal Astronomical Society, 456, 2070.
<http://adsabs.harvard.edu/abs/2016MNRAS.456.2070T>
- Wright, J. T., Cartier, K. M. S., Zhao, M., Jontof-Hutter,
D., & Ford, E. B. 2016, The Astrophysical Journal, 816,
17. <http://adsabs.harvard.edu/abs/2016ApJ...816...17W>
- Zakamska, N. L., & Tremaine, S. 2004, The Astronomical
Journal, 128, 869.
<http://adsabs.harvard.edu/abs/2004AJ....128..869Z>